A design framework for nonlinear iterative learning control and repetitive control
Applied to three mechatronic case studies

Aarnoudse, Leontine; Pavlov, Alexey; Oomen, Tom

DOI
10.1016/j.conengprac.2024.105976

Publication date
2024

Document Version
Final published version

Published in
Control Engineering Practice

Control Engineering Practice 149 (2024) 105976

Contents lists available at ScienceDirect

Control Engineering Practice

journal homepage: www.elsevier.com/locate/conengprac

A design framework for nonlinear iterative learning control and repetitive control: Applied to three mechatronic case studies☆

Leontine Aarnoudse [a,*], Alexey Pavlov [b], Tom Oomen [a,c]

[a] Department of Mechanical Engineering, Control Systems Technology, Eindhoven University of Technology, Eindhoven, The Netherlands
[b] Department of Geoscience and Petroleum, NTNU Norwegian University of Science and Technology, Trondheim, Norway
[c] Delft Center for Systems and Control, Delft University of Technology, Delft, The Netherlands

ARTICLE INFO

Keywords:
Iterative learning control
Repetitive control
Nonlinear Control
Convergent systems

ABSTRACT

Iterative learning control (ILC) and repetitive control (RC) can lead to high performance by attenuating repeating disturbances perfectly, yet these approaches may amplify non-repeating disturbances. The aim of this paper is to achieve both perfect, fast attenuation of repeating disturbances and limited amplification of non-repeating disturbances. This is achieved by including a deadzone nonlinearity in the learning filter, which distinguishes disturbances based on their different amplitudes to apply different learning gains. Convergence conditions for nonlinear ILC and RC are developed, which are used in combination with system measurements in a comprehensive design procedure. Experimental implementation demonstrates fast learning and small errors.

1. Introduction

Iterative learning control (ILC) and repetitive control (RC) are related approaches that can lead to high performance for systems with disturbances that repeat, either over tasks (iteration-invariant) in ILC or periodically within one task (periodic) in RC, by attenuating these disturbances completely. In ILC, a feedforward signal is updated iteratively after each experiment (Bristow, Tharayil, & Alleyne, 2006), and the system resets after each iteration, whereas in RC, a periodic signal generator is included in the closed loop to reject periodic signals without system resets (Longman, 2010). While iteration-invariant or periodic disturbances are attenuated completely, iteration-varying or non-periodic disturbances may be amplified by ILC (Butcher, Karimi, & Longchamp, 2008; Oomen & Rojas, 2017) and RC (Chen & Tomizuka, 2014).

Linear iteration-invariant ILC approaches are subject to trade-offs when reducing the amplification of iteration-varying disturbances, as this often leads to both reduced attenuation of iteration-invariant disturbances (Bristow et al., 2006) and slower convergence (Butcher et al., 2008). Iteration-invariant ILC approaches to reduce amplification of iteration-varying disturbances include using low-pass robustness filters in frequency-domain ILC (Bristow et al., 2006) or weighting of the feedforward signal in lifted norm-optimal ILC (Gunnarsson & Norrlöf, 2001). These approaches reduce the amplification of varying disturbances at certain frequencies, but they also lead to reduced attenuation of iteration-invariant disturbances at those frequencies. A small learning gain, or weighting of the change in input, leads to both a small error and limited amplification of iteration-varying disturbances, but the convergence is slow.

Since linear iteration-invariant ILC strategies are limited in the presence of iteration-varying disturbances, iteration-varying ILC strategies have been introduced. The overview paper (Shen & Wang, 2014) mentions two distinct stochastic ILC approaches that take into account iteration-varying disturbances to determine iteration-varying ILC update laws that are optimal in some sense. The first approach uses a P-type or D-type ILC update based on Kalman filtering, and requires accurate knowledge of the system and the disturbances, see also Saab (2001, 2003). Similar system and disturbance knowledge is used in Deutschmann-Olek, Stadler, and Kugi (2021), which uses a Wiener-filtering approach to find an optimal update based on the expected power-spectral densities of the iteration-invariant and iteration-varying disturbances. The performance of these approaches depends strongly on the accuracy of the system and disturbance models, and tuning for robustness against model uncertainty is challenging. The second approach is based on stochastic approximation and estimates the gradient based on a perturbation experiment (Chen, 2003). This stochastic gradient descent-based method leads to slow convergence, especially when combined with descending step sizes that are needed to ensure convergence. A similar systematic reduction of the learning gain

☆ This work is part of the research programme VIDI with project number 15698, which is (partly) financed by the NWO, Netherlands.
* Corresponding author.
E-mail address: l.i.m.aarnoudse@tue.nl (L. Aarnoudse).

https://doi.org/10.1016/j.conengprac.2024.105976
Received 16 December 2023; Received in revised form 2 April 2024; Accepted 17 May 2024
Available online 30 May 2024

at each iteration is used in Butcher et al. (2008), which uses a model-based update instead of a gradient estimate, but which still leads to slow convergence when limiting the amplification of iteration-varying disturbances. In Oomen and Rojas (2017), a sparse ILC algorithm is presented which leads to time-varying ILC within one trial. The standard norm-optimal ILC criterion is extended by a convex relaxation of the ℓ_0-norm of the input signal to enforce sparsity. This approach achieves both fast convergence and limited amplification of iteration-varying disturbances, but the input update that minimizes the criterion cannot be obtained in closed form. Instead, an optimization problem is solved for each iteration. Therefore, tuning for robustness is challenging in this approach.

Similar to linear iteration-invariant ILC approaches, linear time-invariant (LTI) RC approaches suffer from trade-offs between learning speed, attenuation of periodic disturbances and limited amplification of non-periodic disturbances. RC modifies the closed-loop through a modifying sensitivity, which contains notches that provide local suppression at the frequency of the periodic disturbance and its harmonics. Due to the waterbed effect, the modifying sensitivity exceeds 0 dB at other frequencies, leading to amplification of non-periodic disturbances or disturbances with different periods. Reducing the cut-off frequency of the low-pass robustness filter or decreasing the learning gain (Yeol & Longman, 2008) in RC has similar disadvantages as in ILC. In addition, reducing the learning gain in RC leads to reduced robustness against period variations or uncertainty. Other approaches, including high-order RC (Pipeleers, Demeulenaere, De Schutter, & Swevers, 2008; Steinbuch, Weiland, & Singh, 2007) and optimal model-based RC designed in conjunction with an observer-state feedback controller (De Roover, Bosgra, & Steinbuch, 2000), allow for more extensive trade-offs yet retain these fundamental limitations. Kalman filters may reduce the amplification of non-periodic disturbances (Longman, 2010), yet require complete knowledge of the system model and the periodic disturbance.

Although significant steps have been taken to apply ILC and RC in the presence of both repeating and non-repeating disturbances, at present no approach exists that achieves fast, strong attenuation of repeating disturbances while limiting the amplification of non-repeating disturbances. To address this challenge, this paper develops nonlinear ILC and RC approaches that include nonlinearities in the frequency-domain learning filters. It is shown that under certain design conditions, ILC and RC algorithms with these incrementally sector-bounded nonlinearities converge similar to linear ILC and RC algorithms. Including nonlinearities leads to an additional degree of freedom to improve the performance of ILC and RC. In particular, by choosing a deadzone it is possible to distinguish between non-repeating (either iteration-varying or non-periodic)and repeating (iteration-invariant or periodic) disturbances based on their amplitude characteristics, and apply learning gains that adapt to the type of disturbance. The idea of nonlinear learning filters in ILC and RC relates to variable-gain feedback controllers constructed through nonlinear filters, see, e.g., Heertjes and Steinbuch (2004) and Pavlov, Hunnekens, Wouw, and Nijmeijer (2013). A similar idea has also been applied to lifted ILC (Aarnoudse, Pavlov, & Oomen, 2023b; Heertjes & Tso, 2007), by including a deadzone nonlinearity in the learning filter.

The contribution of this paper consists of the following elements:

- a framework for nonlinear frequency-domain ILC and RC, including convergence conditions;
- a systematic design procedure for ILC and RC with deadzone nonlinearities, including a simulation case study that illustrates the effect of various design parameters; and
- validation of the approach through two experimental case studies on a benchmark system and on an industrial print belt system, which demonstrate fast and strong attenuation of repeating disturbances while limiting the amplification of non-repeating disturbances.

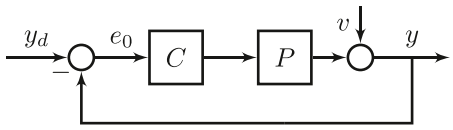

Fig. 1. Closed-loop control scheme.

Preliminary results for nonlinear frequency-domain ILC and RC are presented in respectively Aarnoudse, Pavlov, and Oomen (2023a) and Aarnoudse, Pavlov, Kon, and Oomen (2023). The present paper extends these results by a complete design procedure, extensive simulation results and experimental implementation. In addition, for nonlinear frequency-domain ILC a new convergence theorem is developed that considers iteration-varying inputs.

Related results for lifted ILC are presented in Aarnoudse, Pavlov, and Oomen (2023b), which interprets the nonlinear lifted ILC system as a multiple-input multiple-output (MIMO) Lur'e system in the iteration domain. Convergence criteria are developed by analyzing this system as a discrete-time convergent system (Pavlov & Van De Wouw, 2012). The theoretical results obtained for lifted ILC assume finite-time signals, and cannot be applied directly to frequency-domain ILC, which assumes infinite-time signals. Therefore, in this paper convergence criteria are developed for nonlinear frequency-domain ILC, a corresponding design procedure is provided, and the method is validated experimentally on a benchmark system. In addition, the method is extended to nonlinear repetitive control.

This paper is structured as follows. The problem is formulated in Section 2. Nonlinear ILC and RC algorithms that include a static incremental-sector bounded nonlinearity are introduced, and convergence conditions are developed, in respectively Sections 3 and 4. The amplification of disturbances in ILC and RC is analyzed in Section 5, and a deadzone nonlinearity is introduced to apply adapting gains based on the disturbance amplitude. In Section 6 the design procedure is explained and illustrated using simulation results. The approach is validated experimentally for ILC and RC in Section 7 and conclusions are given in Section 8.

Notation: For a vector x and a matrix P, $\|x\|_2 = \sqrt{\sum_{i=-\infty}^{\infty} |x_i|^2} < \infty$ denotes the ℓ_2-norm for $x \in \ell_2$ and $\|x\|_P = \sqrt{x^\mathsf{T} P x}$ denotes the weighted 2-norm. The spectral radius of a matrix is denoted by $\rho(P)$. The $\mathcal{H}_\infty$-norm is denoted by $\|G\|_\infty = \sup_{\omega\in[0,2\pi)} |G(e^{i\omega})|$ for a real-rational, causal and stable transfer function $G \in \mathcal{RH}_\infty$, and $\|G\|_{\mathcal{L}_\infty} = \sup_{\omega\in[0,2\pi)} |G(e^{i\omega})|$ denotes the $\mathcal{L}_\infty$-norm for a rational transfer function $G \in \mathcal{RL}_\infty$. The sets of real, natural, and integer numbers are denoted by $\mathbb{R}$, $\mathbb{N}$ and $\mathbb{Z}$, respectively. The power spectrum ϕ_x of signal x is defined as in Ljung (1999, Section 2.3).

2. Problem formulation

Consider a single-input single-output (SISO) LTI system as depicted in Fig. 1, with a system P and a feedback controller C. The error of the original closed-loop system, e_0, is given by

$$e_0 = \underbrace{(1 + PC)^{-1}}_{S}(y_d - v), \tag{1}$$

with reference y_d and measurement noise v. Without loss of generality, it is assumed that y_d is either iteration-invariant or periodic, while v is iteration-varying or non-periodic. Since the system is LTI, all other repeating and non-repeating disturbances can be included in the terms Sy_d or Sv, respectively. Depending on whether y_d is repeating over tasks or periodic within one task, either iterative learning control or repetitive control can be used to attenuate the disturbances induced by y_d completely by injecting a compensating signal after the controller in parallel ILC, adding a compensating signal to the reference in serial ILC, or including a periodic signal generator before the controller in

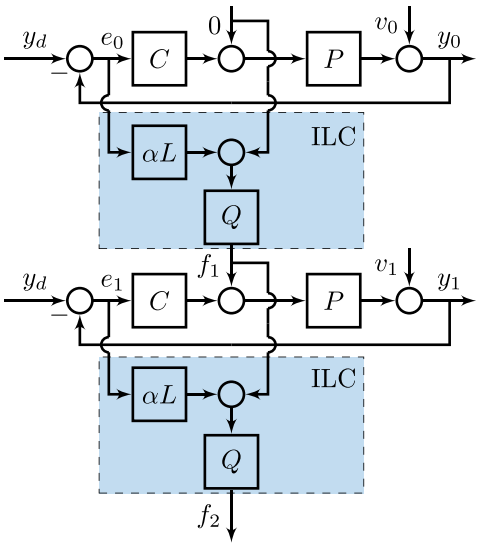

Fig. 2. Parallel iterative learning control scheme with the ILC update indicated in blue.

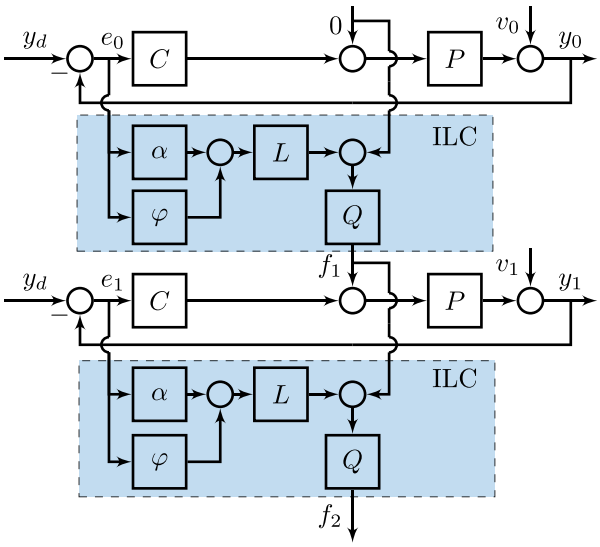

Fig. 3. Nonlinear parallel iterative learning control scheme with deadzone nonlinearity φ. The ILC update is indicated in blue.

RC. The main difference is that in contrast to ILC, RC does not assume a system reset between occurrences of the disturbance. Typical ILC and RC implementations are shown in respectively Figs. 2 and 4.

This paper includes three different case studies on ILC and RC for mechatronic systems that are subject to repeating and non-repeating disturbances. The first is a simulation study using an industrial flatbed printer that performs a scanning motion. The second case study considers an experimental benchmark system that performs a scanning motion similar to the flatbed printer. Third, experiments are performed on an industrial print belt system that consists of various rollers and belts that introduce periodic and non-periodic disturbance while the system rotates with a constant velocity. The problem considered in this paper is the development of ILC and RC approaches for these types of systems, that can attenuate iteration-invariant or periodic disturbances completely in a small number of iterations/periods, without amplifying iteration-varying or non-periodic disturbances. Convergence conditions should be developed for these algorithms, that can be evaluated based on frequency-response measurements in order to design for robustness against model uncertainty in a systematic design procedure.

3. Nonlinear iterative learning control

In this section, nonlinear iterative learning control is introduced. The standard formulations are extended by a sector-bounded nonlinearity, and convergence conditions are developed. In the standard ILC configuration illustrated in Fig. 2, a feedforward signal f_j is applied to the closed-loop system, resulting in the error

$$e_j = S(y_d - v_j) - Jf_j \tag{2}$$

at iteration j. Here $J = SP$ denotes the process sensitivity of the system. Feedforward signal f_j is updated iteratively according to

$$f_{j+1} = Q(f_j + \alpha Le_j), \tag{3}$$

with learning filter L, which is chosen to approximate J^{-1}, robustness filter Q, which is typically a zero-phase low pass filter, and learning gain α which is typically chosen to be $\in (0, 1]$.

In the presented nonlinear ILC approach, the ILC update (3) is extended by a static nonlinearity φ. The motivation for including this type of nonlinearity is that it can increase the design freedom in ILC significantly, while convergence is still ensured under mild conditions that can be evaluated using identified frequency responses of the system. The additional design freedom is exploited in Section 5, where φ is chosen as a deadzone nonlinearity that enables fast convergence to small errors. The static nonlinearity φ satisfies the incremental sector condition

$$0 \leq \frac{\varphi(a) - \varphi(b)}{a - b} \leq \gamma \tag{4}$$

for any two scalars a and b. The nonlinear ILC scheme is illustrated in Fig. 3 and uses the feedforward update

$$f_{j+1} = Q(f_j + \alpha Le_j + L\varphi(e_j)), \tag{5}$$

To analyze the convergence of algorithm (5) in case of frequency-domain ILC, consider the following feedforward and error iterations

$$\begin{aligned} f_{j+1} = {} & \alpha QLS(y_d - v_j) + Q(1 - \alpha LJ)f_j \\ & + QL\varphi(S(y_d - v_j) - Lf_j), \end{aligned} \tag{6}$$

$$\begin{aligned} e_{j+1} = {} & (1 - Q)Sy_d + QSv_j - Sv_{j+1} \\ & + Q(1 - \alpha JL)e_j - QJL\varphi(e_j). \end{aligned} \tag{7}$$

The feedforward and error iterations for nonlinear ILC are interpreted as nonlinear systems in the iteration domain. To analyze the stability of nonlinear ILC and RC with iteration-varying or non-periodic inputs, the notion of exponential convergence for nonlinear systems is introduced (Pavlov & Van De Wouw, 2012, Definition 1).

Definition 1. The system

$$x(k + 1) = h(x(k), k), \tag{8}$$

with state $x \in \mathbb{R}^n$, $h : \mathbb{R}^n \times \mathbb{Z} \to \mathbb{R}^n$ and discrete-time variable $k \in \mathbb{Z}$, is called exponentially convergent if

- there exists a unique solution $\bar{x}(k)$ that is defined and bounded on $\mathbb{Z}$ (from $-\infty$ to $+\infty$),
- $\bar{x}(k)$ is globally exponentially stable, i.e., there exists $c > 0$ and $0 < \lambda < 1$ such that $|x(k) - \bar{x}(k)| \leq c\lambda^{k-k_0}|x(k_0) - \bar{x}(k_0)|$ for all $k \geq k_0$.

Solution $\bar{x}(k)$ is called a steady-state solution, to which any solution of the convergent system converges, irrespective of the initial condition. The time dependency of (8) is typically due to an input, and if that input is periodic then $\bar{x}$ is periodic with the same period (Pavlov & Van De Wouw, 2012). If the right-hand side of (8) is independent of time, then the steady-state solution is constant. The convergence property is an extension of the stability properties of asymptotically

stable linear systems excited by external inputs. The following result establishes exponential convergence of a nonlinear system (Pavlov & Van De Wouw, 2012, Theorem 1).

Lemma 2. *Consider system (8) with a Lipschitz continuous (Khalil, 2002, Chapter 3) right-hand side satisfying*

$$\|h(x_1,k)-h(x_2,k)\|_P \le \lambda\|x_1-x_2\|_P, \quad \forall x_1,x_2\in\mathbb{R}^n, k\in\mathbb{Z} \tag{9}$$

$$\sup_{k\in\mathbb{Z}}\|h(0,k)\|_P < +\infty, \tag{10}$$

for some matrix $P=P^{\mathsf{T}}\succ 0$ and number $\lambda\in(0,1)$. Then system (8) is exponentially convergent.

The notion of monotonic convergence in the ℓ_2-norm of the sequence of iterates is commonly used in ILC to ensure good learning transients (Longman, 2000). This notion relates to the notion of exponential convergence as used for the analysis of nonlinear systems according to the following definition.

Definition 3. A system (8) is called monotonically exponentially convergent if it satisfies the conditions of Lemma 2 with $P=I$. In that case, the corresponding sequence of states $\{x(k)\}$ converges monotonically in the ℓ_2-norm $\|x\|_2=\sqrt{\sum_{-\infty}^{\infty}|x_i|^2}<\infty$.

A condition for the monotonic exponential convergence of the error iteration (7) in frequency domain ILC is given by the following theorem for an invertible system J.

Theorem 4. *The error iteration (7) for system (2) with feedforward update (5) and nonlinearity φ satisfying (4) is monotonically exponentially convergent if*

$$\left\|Q\left(1-\left(\alpha+\frac{\gamma}{2}\right)JL\right)\right\|_{\mathcal{L}_\infty}+\frac{\gamma}{2}\|QJL\|_{\mathcal{L}_\infty}<1, \tag{11}$$

with $\gamma,\alpha>0$. Then the corresponding sequence of iterates $\{e_j\}$ converges monotonically in the ℓ_2-norm to a unique steady-state solution $\bar{e}_j$.

The proof of Theorem 4 is given in the appendix. Note that while Theorem 4 employs the same notion of discrete-time convergent systems as used in Aarnoudse, Pavlov, and Oomen (2023b, Theorem 9) for lifted ILC, the resulting convergence conditions are different. Both approaches analyze the mapping from signals of one iteration to the next, but Theorem 4 analyzes the mapping directly using frequency-domain filters, whereas Aarnoudse, Pavlov, and Oomen (2023b, Theorem 9) considers the lifted ILC system as a MIMO Lur'e system in the iteration domain for which finally a MIMO frequency-domain condition is obtained. The convergence conditions for nonlinear frequency-domain ILC and lifted ILC cannot be interchanged.

Since the system J in frequency-domain ILC is a transfer function, the inverse J^{-1} exists. Therefore, substitutions of the form $f_j=J^{-1}(S(y_d-v_j)-e_j)$ are possible and monotonic convergence of the sequence of error iterates ensures convergence of the sequence of feedforward iterates. Note that if J^{-1} contains poles outside of the unit disc due to non-minimum phase zeros in J, it may be interpreted as a non-causal operator due to the availability of f_j and e_j, see, e.g., Sogo (2010). Regarding the monotonic convergence of the feedforward iteration (6), the following holds.

Theorem 5. *The feedforward iteration (6) for system (2) with feedforward update (5) and nonlinearity φ satisfying (4) is monotonically exponentially convergent if*

$$\left\|Q\left(1-\left(\alpha+\frac{\gamma}{2}\right)JL\right)\right\|_{\mathcal{L}_\infty}+\frac{\gamma}{2}\|QL\|_{\mathcal{L}_\infty}\|J\|_{\mathcal{L}_\infty}<1, \tag{12}$$

with $\gamma,\alpha>0$. Then the corresponding sequence of iterates $\{f_j\}$ converges monotonically in the ℓ_2-norm to a unique steady-state solution $\bar{f}_j$.

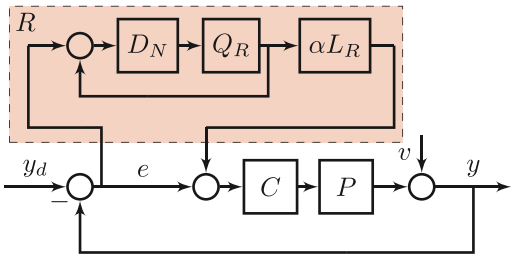

Fig. 4. Repetitive control scheme with the repetitive controller R indicated in red.

The proof of Theorem 5 follows along the same lines as the proof of Theorem 4 in the appendix. The main difference between the conditions in Theorems 4 and 5 is the occurrence of respectively $\|QJL\|_{\mathcal{L}_\infty}$ or $\|QL\|_{\mathcal{L}_\infty}\|J\|_{\mathcal{L}_\infty}$. Since $\|QJL\|_{\mathcal{L}_\infty}\le\|QL\|_{\mathcal{L}_\infty}\|J\|_{\mathcal{L}_\infty}$, if (12) in Theorem 5 holds then (11) in Theorem 4 holds also.

Remark 6. The conditions for monotonic convergence in Theorems 4 and 5 involve $\mathcal{L}_\infty$-norms of dynamical systems. Since

$$\|QJL\|_{\mathcal{L}_\infty}=\sup_{\omega\in[0,2\pi)}|Q(e^{i\omega})J(e^{i\omega})L(e^{i\omega})|, \tag{13}$$

and similarly for the other $\mathcal{L}_\infty$-norms, these conditions can be evaluated based on models or frequency response measurements of J. This is illustrated in Section 6.

Remark 7. The results of Theorems 4 and 5 guarantee monotonic exponential convergence to a steady-state solution for any nonlinearity φ that satisfies the incremental sector condition (4). The selection of φ to improve the performance in the presence of iteration-varying and iteration-invariant disturbances is illustrated in Section 5.

4. Nonlinear repetitive control

In this section, nonlinear RC is introduced and stability conditions are developed. A repetitive controller is a closed-loop controller that is typically implemented as shown in Fig. 4. Consider once again the error e_0 without ILC or RC in (1). Through application of an repetitive controller R, the error is modified to

$$\begin{aligned} e &= (1+PC(1+R))^{-1}(y_d-v) \\ &= \underbrace{(1+TR)^{-1}}_{S_R}e_0, \end{aligned} \tag{14}$$

with $T=\frac{PC}{1+PC}$, see, e.g., Chang, Suh, and Kim (1995) for a derivation. The repetitive controller R is given by

$$R(z)=\frac{\alpha L_R(z)z^{-N}Q_R(z)}{1-z^{-N}Q_R(z)}, \tag{15}$$

with z^{-N} the z-domain representation of the delay operator D_N, such that $D_N(z)=z^{-N}$, which acts as a buffer storing the error signal of the previous repetition. The length of the delay $N\in\mathbb{N}$ corresponds to a disturbance frequency $f_d=f_s/N$ for sampling frequency f_s. Analogous to ILC, the robustness filter $Q_R(z)\in\mathcal{R}$ and learning filter $L_R(z)\in\mathcal{R}$ can be non-causal as long as $R(z)\in\mathcal{RH}_\infty$, i.e., the filters can have finite preview which is compensated by embedding the preview in the delay z^{-N}. Typically, L_R is chosen to approximate T^{-1} using zero-phase error tracking control (ZPETC) (Tomizuka, 1987) and Q_R is a zero-phase low-pass filter. This leads to the modifying sensitivity

$$S_R(z)=\frac{1-z^{-N}Q_R(z)}{1-z^{-N}Q_R(z)(1-T(z)\alpha L_R(z))}. \tag{16}$$

Analogous to nonlinear ILC, a static sector-bounded nonlinearity that satisfies (4) is included in the repetitive controller. The resulting

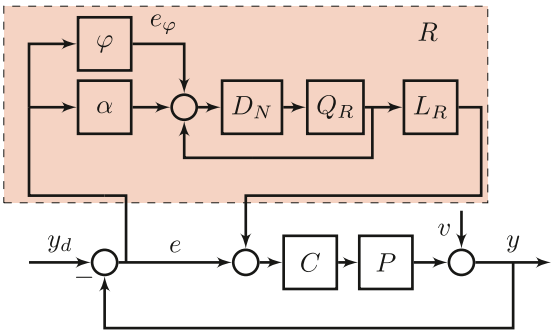

Fig. 5. Nonlinear repetitive control scheme with deadzone nonlinearity φ. The repetitive controller is indicated in red.

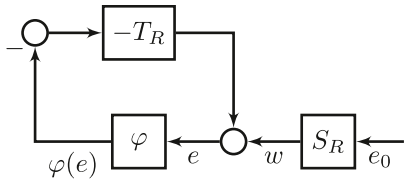

Fig. 6. Nonlinear repetitive control as a Lur'e system.

nonlinear repetitive controller is illustrated in Fig. 5. The input e of the nonlinearity is a function of its output signal $e_\varphi = \varphi(e)$ and the disturbances contained in e_0, such that

$$e = T_R e_\varphi + S_R e_0, \tag{17}$$

in which the complementary sensitivity of the linear RC loop is given by

$$T_R = \frac{TR}{1+TR}. \tag{18}$$

RC is implemented as a feedback controller, which can influence the stability of the closed-loop system. In contrast, ILC is implemented with resets after each iteration, which means that stability or convergence only needs to be analyzed in the iteration domain. Since for traditional (linear) RC stability of the closed-loop time-domain system is desired (Longman, 2010), for nonlinear RC convergence according to Definition 1 is shown.

To analyze the existence and global exponential stability of the steady-state solution of the nonlinear RC system (17), it is rewritten in state-space form as a cascade of a linear system S_R and a Lur'e system formed by the linear system $-T_R$ with static nonlinearity φ in feedback, see Fig. 6. The dynamics of the cascaded system are given by

$$\left.\begin{aligned} x(k+1) &= Ax(k)+Bu(k)\\ y(k) &= Cx(k)\end{aligned}\right\} -T_R \tag{19a}$$

$$u(k) = -\varphi(y(k)+w(k))$$

$$\left.\begin{aligned} n(k+1) &= An(k)+Be_0(k)\\ w(k) &= Cn(k)+e_0(k)\end{aligned}\right\} S_R \tag{19b}$$

The matrices A, B and C form a minimal state-space realization of $-T_R$, such that (A,B) is controllable and (A,C) is observable. Note that since $S_R = 1 - T_R$, (19a) and (19b) have the same A, B and C-matrices. For the convergence of the nonlinear RC system, the following theorem holds.

Theorem 8. *Given a minimal realization (A,B,C) of the linear system $-T_R$ with (A,B) controllable and (A,C) observable. The nonlinear RC system (19) is exponentially convergent for any input $e_0(k)$ bounded on $\mathbb{Z}$ if the following conditions are met:*

(a) $\rho(A) < 1$.

(b) φ *satisfies (4) for a certain* γ.

(c) The following small-gain condition holds:

$$\sup_{\omega\in[0,2\pi)} |T_R(e^{i\omega})| < \frac{1}{\gamma}. \tag{20}$$

The proof is given in the appendix. Condition (a) of Theorem 8 can be satisfied through the design of L and Q, similar to ILC, as stability of the linear system can be verified using identified frequency response functions of the system. Similarly, condition (c) is satisfied by choosing suitable values for the linear gain α and the nonlinear gain γ, and can be verified using a measured frequency response.

Remark 9. Theorem 8 provides conditions for exponential convergence for any nonlinearity φ that satisfies the incremental sector condition (4). How to select φ to improve the performance of nonlinear RC in the presence of periodic and non-periodic disturbances is described in the next section.

5. Nonlinear ILC and RC for fast convergence and high accuracy

In the previous two sections, nonlinear ILC and RC are introduced. In this section the propagation of disturbances in ILC and RC is illustrated, and it is shown how the LTI design parameters influence the attenuation and amplification of the disturbances. Finally, a nonlinear filter is introduced to reduce the amplification of non-repeating disturbances and achieve both fast convergence and high performance through nonlinear ILC and RC.

5.1. Amplification of iteration-varying disturbances in ILC

Consider the ILC system (2) with update (3). To analyze the propagation of the iteration-invariant and iteration-varying disturbances Sy_d and Sv_j over iterations, it is assumed that Q and L are chosen such that the sequence of error iterates $\{e_j\}$ is convergent. In addition, assume that v_j is i.i.d. zero-mean white noise and S is monic and bistable (Ljung, 1999). Then, for $f_0 = 0$ and $j \to \infty$, the spectrum of the converged error is given by Oomen and Rojas (2017, Theorem 3)

$$\phi_{e_\infty} = \left|\frac{1-Q}{1-Q(1-\alpha LJ)}\right|^2 \phi_{Sy_d} + \left(1+\frac{|\alpha JQL|^2}{1-|Q(1-\alpha LJ)|^2}\right)\phi_{Sv}, \tag{21}$$

with ϕ_{Sy_d} and ϕ_{Sv} the spectra of the iteration-invariant disturbance Sy_d and the iteration-varying disturbance Sv, respectively. For the simple case with $Q = 1$ and $L = J^{-1}$, it is clear that the first term in (21) is equal to zero, such that the spectrum of the resulting converged error is given by

$$\phi_{e_\infty} = \left(1+\frac{\alpha^2}{2\alpha-\alpha^2}\right)\phi_{Sv}. \tag{22}$$

For learning gain $\alpha = 1$, this gives $\phi_{e_\infty} = 2\phi_{Sv}$, i.e., the iteration-varying part of the error is amplified by a factor 2 by ILC. For $\alpha \to 0$, this effect is mitigated and $\phi_{e_\infty} \to \phi_{Sv}$. This is the smallest achievable spectrum, since ILC cannot compensate for the unknown iteration-varying disturbance Sv_j in iteration j.

While reducing α reduces the spectrum of the converged error, it also reduces the convergence speed significantly. In addition, reducing $\alpha \in (0,1]$ when $Q \neq 1$ may increase the contribution of the spectrum of the iteration-invariant disturbance to the error. To illustrate this, consider the case with $Q \neq 1$ and $L = J^{-1}$, such that

$$\phi_{e_\infty} = \left|\frac{1-Q}{1-Q(1-\alpha)}\right|^2 \phi_{Sy_d} + \left(1+\frac{|\alpha Q|^2}{1-|Q(1-\alpha)|^2}\right)\phi_{Sv}. \tag{23}$$

In this case reducing $\alpha \in (0,1]$ reduces the term $1-Q(1-\alpha)$ in the numerator of the term before ϕ_{Sy_d}, thus increasing the contribution of

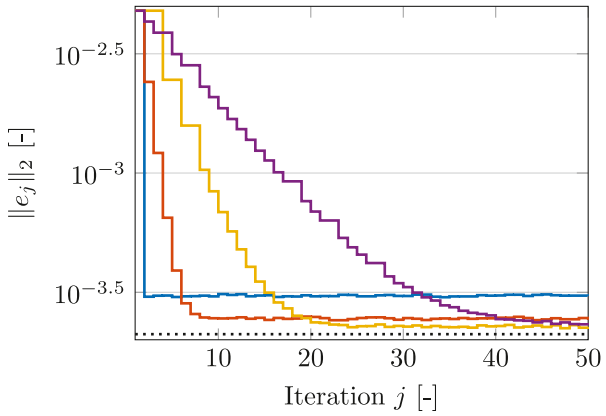

Fig. 7. Error 2-norm over iterations for $\alpha = 1$ (—), 0.5 (—), 0.2 (—) and 0.1 (—), and the noise floor (·····), averaged over 20 realizations. Small learning gains lead to lower converged errors at the cost of slower convergence. (For interpretation of the references to color in this figure legend, the reader is referred to the web version of this article.)

$\phi_{S y_d}$ to ϕ_{e_∞}. It is therefore, in general, not desired to choose $\alpha \approx 0$. In Fig. 7 the effect of reducing α is illustrated using simulation results that are further elaborated upon in Section 6. It is shown that for high values of α, the convergence is fast but the converged error is relatively high. Reducing the learning gain reduces results in slow convergence, but the converged error is reduced significantly since iteration-varying disturbances are amplified less.

Analysis of the modifying sensitivity S_R in (16) shows that repetitive control suffers from a similar trade-off between convergence speed and converged error as ILC when both periodic and non-periodic disturbances are present (Aarnoudse, Pavlov, Kon, & Oomen, 2023). This is illustrated in a simulation example in Section 6.5. Reducing the learning gain α leads to reduced amplification of non-periodic disturbances, but it also reduces the period-robustness of the repetitive controller, which is problematic if f_d is not known exactly. In addition, if α is reduced more periods are needed to attenuate the periodic disturbance.

5.2. Adapting learning gains through a deadzone nonlinearity

The nonlinearity included in the ILC and RC algorithms in Sections 3 and 4 can be employed to apply different learning gains based on the type of disturbances in the error signal. In particular, a deadzone nonlinearity is included in ILC and RC to apply different learning gains to samples of the error signal based on the amplitude characteristics, where it is assumed that repeating disturbances have, in general, larger amplitudes than non-repeating disturbances. The deadzone, which is a static nonlinearity that satisfies the incremental sector condition (4), is illustrated in Fig. 8. It is applied to each element of e according to

$$\varphi(e(k)) = \begin{cases} 0, & \text{if } |e(k)| \leq \delta \\ (\gamma - \frac{\gamma\delta}{|e(k)|})e(k), & \text{if } |e(k)| > \delta. \end{cases} \tag{24}$$

The width of the deadzone is denoted by δ, and γ is a nonlinear learning gain that can be compared to the linear learning gain α in (3) and (15), in the sense that it influences the convergence speed and the amplification of iteration-varying disturbances. The main idea is that learning is only applied to the error values that are above the threshold δ, where δ is chosen such that $\varphi(v_j) \approx 0$. This allows for fast convergence when the error is large, while disturbance amplification is limited when the error is small. The width δ of the deadzone can be chosen based on knowledge of the iteration-varying disturbances, as explained in Section 6.

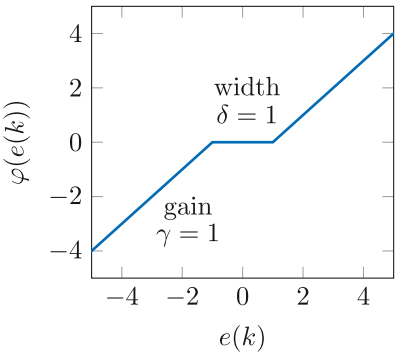

Fig. 8. Deadzone nonlinearity φ according to (24) with width $\delta = 1$ and gain $\gamma = 1$.

6. Design procedure and illustrative example

In this section, a design procedure using system measurements is presented and illustrated through a case study on an industrial flatbed printer. First, filters L and Q are designed using standard approaches for frequency-domain ILC or RC. Then, the gains α and γ are chosen. Lastly, the width of the deadzone nonlinearity is determined based on a series of experiments. The design procedure for nonlinear ILC is summarized in Procedure 10. For nonlinear RC, the same strategy is employed to determine α, γ and deadzone width δ, as summarized in Procedure 11. The design procedure in this section is only illustrated for nonlinear ILC for conciseness, since the procedure for RC is similar. At the end of this section, it is explained where the RC procedure differs from ILC, and a simulation example for nonlinear RC is provided.

Procedure 10 Nonlinear ILC design

1: Design learning filter L to approximate J^{-1} (Section 6.2).
2: Design robustness filter Q such that $\|Q(1 - JL)\|_{\mathcal{L}_\infty} < 1$ (Section 6.2).
3: Choose γ such that $\frac{\gamma}{2}\|QJL\|_{\mathcal{L}_\infty} < 0.5$ (Section 6.3).
4: Choose α small, while meeting the convergence condition in Theorem 4 (Section 6.3).
5: Determine deadzone width δ based on system measurements (Section 6.4).

Procedure 11 Nonlinear RC design

1: Design learning filter L_R to approximate T^{-1} (Section 6.2).
2: Design robustness filter Q_R such that $\|Q_R(1 - TL_R)\|_\infty < 1$ (Section 6.2).
3: Choose $\gamma \approx 1$ and α small, while ensuring that the convergence conditions in Theorem 8 are met (Section 6.3).
4: Determine deadzone width δ based on system measurements (Section 6.4).

6.1. Case 1: nonlinear ILC on an industrial flatbed printer

To illustrate the various steps of the design procedure, a case study using simulations of the carriage of an industrial flatbed printer is included. In this case study the focus is on nonlinear ILC, which is a suitable control strategy for many standard printing tasks, yet specific tasks such as continuous media flow printing would also motivate the use of RC, see, e.g., Blanken, Koekebakker, and Oomen (2020). Here, the true system P is a 20th-order model of the carriage, which is approximated by a 12th-order model $\hat{P}$. At high frequencies, there is a model mismatch between P and $\hat{P}$, see Fig. 9. The system is placed in feedback with a PD-type controller C. The fourth-order reference consists of a forward and backward translation and in the simulations Gaussian white noise with a variance of 0.005 is added to the plant

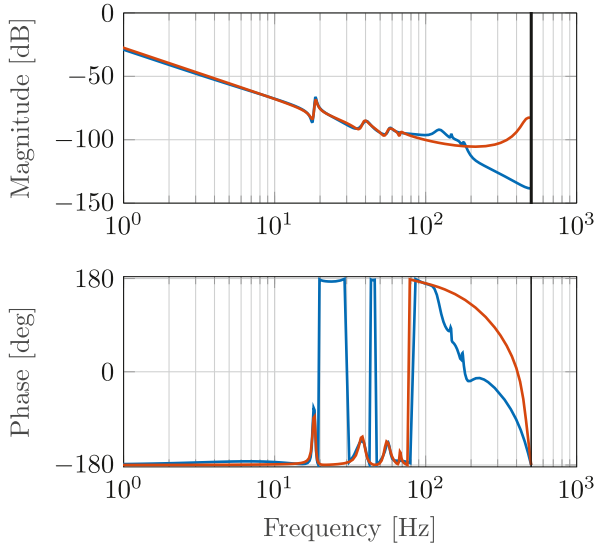

Fig. 9. Bode diagram of the 'true' simulated system P (—) and a low-order approximation $\hat{P}$ (—). (For interpretation of the references to color in this figure legend, the reader is referred to the web version of this article.)

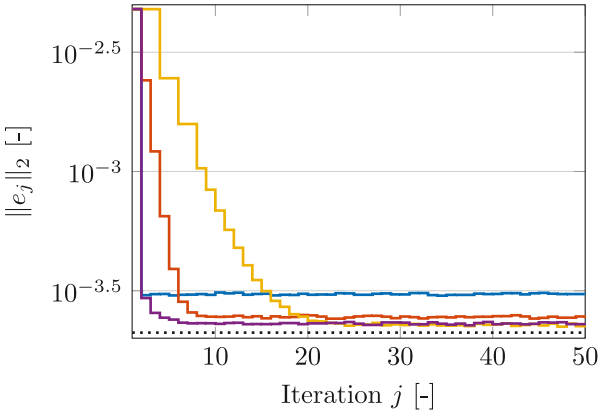

Fig. 10. Error 2-norm for linear ILC with $\alpha = 1$ (—), 0.5 (—) and 0.2 (—) and nonlinear ILC with $\alpha = 0.1$, $\gamma = 0.9$ and $\delta = 5 \times 10^{-6}$ (—). The noise floor (·····) follows from the averaged 2-norm of ten noise realizations. Nonlinear ILC removes the trade-off between convergence speed and converged error. (For interpretation of the references to color in this figure legend, the reader is referred to the web version of this article.)

input. Nonlinear parallel ILC is applied as shown in Fig. 3, such that $J = \frac{P}{1+PC}$ and $\hat{J} = \frac{\hat{P}}{1+\hat{P}C}$. For each ILC configuration, the results are averaged over 20 realizations.

Fig. 10 shows simulation results for nonlinear ILC based on the design procedure that is explained in the remainder of this section. The results illustrate that nonlinear ILC removes the trade-off between convergence speed and converged error value, achieving both fast convergence and small converged errors. In contrast, for linear ILC, smaller values of $0 < \alpha \leq 1$ result in slower convergence and lower errors, as explained in Section 2.

6.2. Design of Q and L for ILC

The convergence conditions of Theorems 4 and 5 resemble the standard convergence conditions for frequency-domain ILC and can be evaluated using frequency response measurements of J. This is advantageous for mechatronic systems, because these measurements are typically fast, inexpensive and give accurate system information. The following design procedure is used to select Q and L, where the selection of α and γ is left out on purpose.

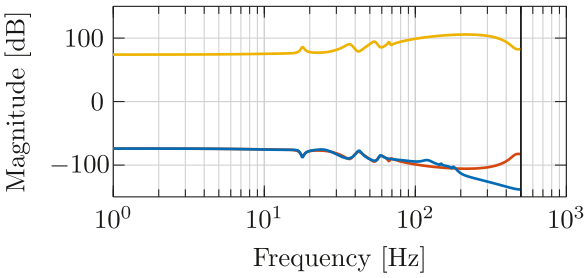

Fig. 11. Bode magnitude plots of J (—), $\hat{J}$ (—) and $L = \hat{J}^{-1}$ (—), obtained using stable inversion. (For interpretation of the references to color in this figure legend, the reader is referred to the web version of this article.)

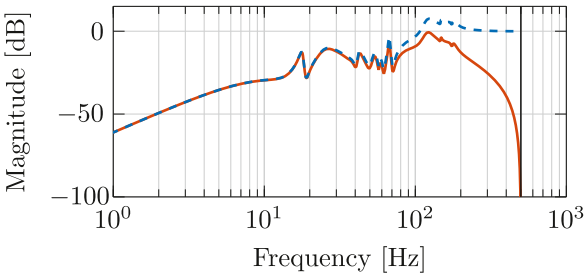

Fig. 12. Bode magnitude plots of $1 - JL$ (- -) and $Q(1 - JL)$ (—). The first-order lowpass filter Q is designed such that $\|\tilde{Q}(1 - \tilde{J}\tilde{L})\|_{\mathcal{L}_\infty} < 1$.. (For interpretation of the references to color in this figure legend, the reader is referred to the web version of this article.)

1. Determine a parametric model $\hat{J}$ of J and obtain measured or model-based frequency-response data of J. Then, choose $L = \hat{J}^{-1}$. Note that by using stable inversion, see e.g. Sogo (2010), $\hat{J}$ can be inverted exactly even if it is non-minimum phase. Alternatively, techniques like ZPETC (Tomizuka, 1987) give $L \approx \hat{J}^{-1}$. This step is illustrated for the simulation example in Fig. 11, where stable inversion is used.
2. Plot the Bode magnitude diagram of $1 - JL$ and determine the frequencies where $|1 - J(e^{i\omega})L(e^{i\omega})| \geq 1$. Design Q such that it is as close to 1 as possible, while making sure that $\|Q(1-JL)\|_{\mathcal{L}_\infty} < 1$. Since Q may be non-causal and computations are offline, it is advantageous to choose it as a zero-phase filter $Q = Q_p^* Q_p$. This step is illustrated for the simulation example in Fig. 12, where the Q-filter is chosen as a first-order lowpass filter with a cutoff frequency of 100 Hz.

These steps leads to a design that meets the convergence condition for $\alpha = 1$, $\gamma = 0$, which does not yet include any nonlinear components. This provides a basis for selecting suitable values of α and γ. In the remainder of this section, stable inversion (Sogo, 2010) is used such that $L = \hat{J}^{-1}$ and the Q-filter is chosen as a first-order lowpass filter with a cutoff frequency of 100 Hz.

6.3. Nonlinear gain selection for ILC

The main idea of using a nonlinear learning filter in ILC and RC is that when δ is chosen such that $\varphi(v_j) \approx 0$, the nonlinear learning gain γ affects only the repeating part of the disturbances and can be chosen close to 1 to enable fast learning, while the linear learning gain α affects both the repeating and non-repeating disturbances and should be chosen ≈ 0 to ignore the non-repeating disturbances completely. However, non-repeating disturbances may occur on top of repeating disturbances for part of the experiment, as seen in Fig. 16. In this region, the deadzone nonlinearity acts as an automatic gain-tuner. Initially, the error exceeds the deadzone bound, such that the nonlinear learning gain γ leads to fast attenuation of the repeating disturbances,

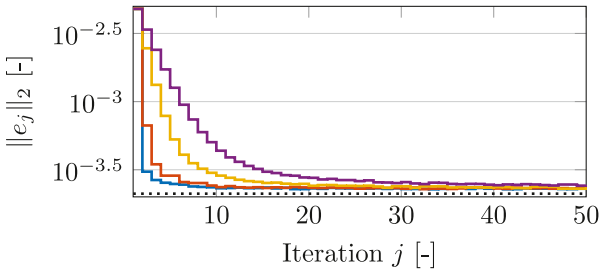

Fig. 13. Error 2-norm over iterations for $\alpha = 0.01$, $\delta = 6\times10^{-6}$ and varying values of γ: $\gamma = 1$ (—), 0.9 (—), 0.5 (—) and 0.3 (—), and the noise floor (·····), averaged over 20 realizations. High nonlinear gains lead to both small errors and fast convergence, and decreasing the gain does not decrease the converged error further. (For interpretation of the references to color in this figure legend, the reader is referred to the web version of this article.)

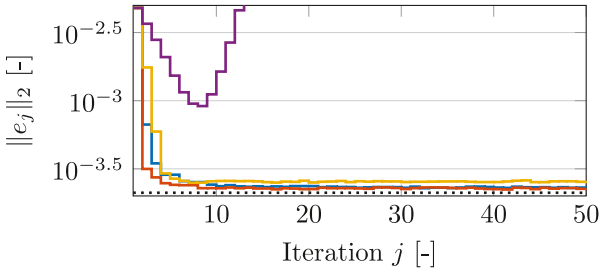

Fig. 14. Error 2-norm over iterations for $\gamma = 0.9$, $\delta = 6\times10^{-6}$ and varying values of α: $\alpha = 0.01$ (—), 0.1 (—), 0.5 (—) and 0.9 (—), and the noise floor (·····), averaged over 20 realizations. Small linear gains lead to fast convergence and low errors, while increasing the linear gain increases the error and may lead to diverging behavior (—). (For interpretation of the references to color in this figure legend, the reader is referred to the web version of this article.)

yet the non-repeating disturbances are amplified. As the repeating disturbances are attenuated the total error approaches the bounds of the deadzone. At that point, the relative influence of α increases and if α is small, the initial amplification is reduced. At this point the convergence speed and converged error depend on α.

Simulation results show that α should be small but nonzero, while γ should be close to 1. Fig. 13 illustrates the influence of deadzone gain γ for $\gamma \in \{0.3, 0.5, 0.9, 1\}$, $\alpha = 0.01$ and $\delta = 6\times10^{-6}$. Increasing γ increases the convergence speed but not the converged error. Therefore, γ should be chosen as close to 1 as possible while still ensuring convergence. Fig. 14 illustrates the influence of linear gain α for $\alpha \in \{0.01, 0.1, 0.5, 0.9\}$, $\gamma = 0.9$ and $\delta = 6\times10^{-6}$. For small values of α, further reducing it slightly reduces the convergence speed and barely influences the converged error. Choosing α too high leads to increased converged errors or even divergence. In general, α should be chosen small but nonzero. In some of the combinations compared in this section, $\alpha + \gamma > 1$, which may lead to increased amplification of non-repeating disturbances (cf. Eq. (22)) and reduced convergence speed, as is also seen in Fig. 14. But since the effective gain of the nonlinear ILC algorithm depends also on the deadzone width and the error magnitude, it is not necessarily problematic if the sum of $\alpha+\gamma > 1$, see, e.g., Fig. 13 for $\alpha = 0.01$ and $\gamma = 1$.

Both γ and α also influence the stability criteria, which should be taken into account. In particular, the convergence condition often limits how small α may be. The gains can be chosen as follows for frequency-domain ILC:

1. Choose γ such that $\frac{\gamma}{2}\|QJL\|_{\mathcal{L}_\infty} < 1$ or such that $\frac{\gamma}{2}\|QL\|_{\mathcal{L}_\infty}\|J\|_{\mathcal{L}_\infty} < 1$, depending on whether the condition for the error iteration or the feedforward iteration is used. Typically, the idea is to combine a value of γ close to 1 with a small value α. To that end, it is desirable that $\frac{\gamma}{2}\|QJL\|_{\mathcal{L}_\infty}$ respectively $\frac{\gamma}{2}\|QL\|_{\mathcal{L}_\infty}\|J\|_{\mathcal{L}_\infty} < 0.5$.
2. Choose α small, but such that the convergence condition in Theorems 4 or 5 is met. Fig. 15 shows the Bode magnitude diagrams of the two terms $\frac{\gamma}{2}QJL$ and $Q\left(1-\alpha JL-\frac{\gamma}{2}JL\right)$ in the convergence condition of Theorem 4 for the simulation example with $\alpha = 0.3$ and $\gamma = 0.7$.

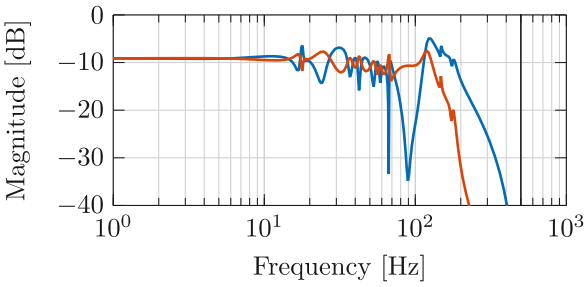

Fig. 15. Bode magnitude plots of $Q\left(1-\alpha JL-\frac{\gamma}{2}JL\right)$ with $\mathcal{L}_\infty = 0.5720$ (—) and $\frac{\gamma}{2}QJL$ with $\mathcal{L}_\infty = 0.4224$ (—). Since $0.5720 + 0.4224 < 1$, the system with $\alpha = 0.3$, $\gamma = 0.7$ meets the convergence condition of Theorem 4. (For interpretation of the references to color in this figure legend, the reader is referred to the web version of this article.)

6.4. Deadzone selection for ILC

The aim is to attenuate repeating disturbances completely, without amplifying the non-repeating disturbances. To choose the deadzone width δ appropriately, it is therefore important to determine the size of the non-repeating disturbances. To this end, consider a series of n_e experiments on the system (2) with $f_j = 0\ \forall\ j$. The output of each experiment is given by

$$e_j = Sy_d - Sv_j \tag{25}$$

with Sy_d the iteration-invariant part of the disturbances, and Sv_j a realization of the iteration-varying disturbances. Note that Sv_j is by definition zero-mean, since any bias is iteration-invariant which means that it is included in Sy_d. An estimate $\widehat{Sy_d}$ of the invariant part of the disturbances is obtained by computing the sample mean of the error signal over n_e experiments, see also Oomen (2020):

$$\widehat{Sy_d} = \frac{1}{n_e}\sum_{j=0}^{n_e-1} e_j = Sy_d - \frac{1}{n_e}\sum_{j=0}^{n_e-1} Sv_j. \tag{26}$$

Then, for each experiment e_j an estimate of the iteration-varying disturbances is given by

$$\widehat{Sv}_j = \widehat{Sy_d} - e_j. \tag{27}$$

This gives several realizations of the iteration-varying part of the error. Based on the distribution of these disturbances, a suitable value of δ that filters out the desired percentage of iteration-varying disturbances can be chosen. Note that for values slightly larger than δ the gain is very small, because of the shape of the deadzone, see Fig. 8. Therefore, it is typically not necessary to choose δ so high that all iteration-varying disturbances are included. The estimates $\widehat{Sy_d}$, $\widehat{Sv_j}$ and the intervals corresponding to $\delta = 3\times10^{-6}$, 5×10^{-6}, and 8×10^{-6}, are illustrated in Fig. 16 for $n_e = 20$.

Fig. 17 illustrates the influence of the deadzone width δ for $\delta \in \{3, 4, 5, 6, 7, 8\}\times10^{-6}$, $\alpha = 0.01$ and $\gamma = 1$. Here, $\delta = 5\times10^{-6}$ leads to the best performance in terms of convergence speed and converged error. If δ is small compared to the noise level, many iteration-varying disturbances exceed the deadzone resulting in larger errors. Similarly, if α is too large, the part of the iteration-invariant disturbances that is not compensated increases which again results in increased errors. In

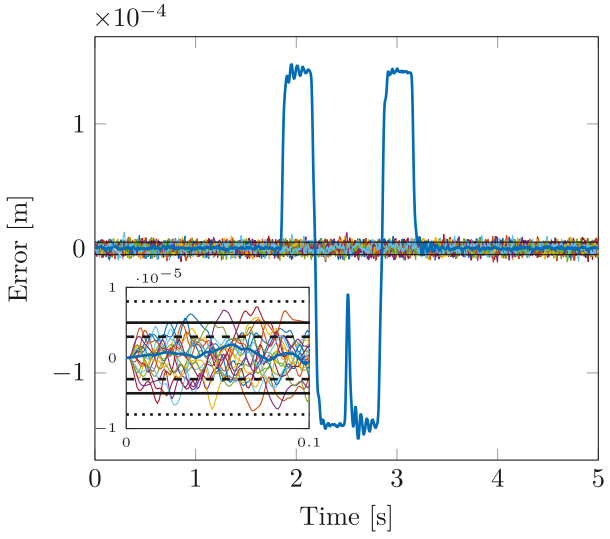

Fig. 16. Mean $\widehat{Sy_d}$ of the error signal over 20 iterations (—) and the noise estimates $\widehat{Sv}_j$ for $j = 1, 2, \ldots, 20$ in simulation. The black lines indicate three different intervals: $[-3\times10^{-6}, 3\times10^{-6}]$ (- -), $[-5\times10^{-6}, 5\times10^{-6}]$ (—), and $[-8\times10^{-6}, 8\times10^{-6}]$ (·····), which are compared in simulation. (For interpretation of the references to color in this figure legend, the reader is referred to the web version of this article.)

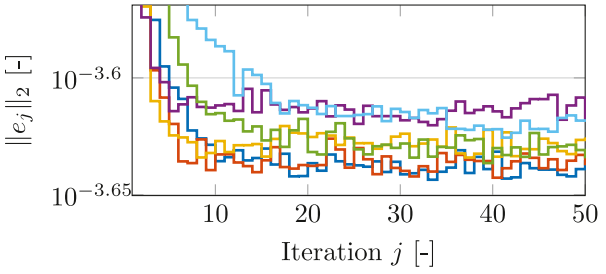

Fig. 17. Error 2-norm over iterations (zoomed in) for $\alpha = 0.01$, $\gamma = 1$ and varying values of δ: $\delta = 3\times10^{-6}$ (—), 4×10^{-6} (—), 5×10^{-6} (—), 6×10^{-6} (—), 7×10^{-6} (—) and 8×10^{-6} (—t), averaged over 20 realizations. The optimal deadzone width is around 5×10^{-6} (—). Even though the differences are small, it is shown that increasing the width leads to larger errors and slower convergence (—,—t), while decreasing the width leads to increased errors with similarly fast convergence (—, —). (For interpretation of the references to color in this figure legend, the reader is referred to the web version of this article.)

addition, increasing δ decreases the convergence speed. It follows that there is an optimal value of δ, and it should be chosen to include most of the iteration-varying disturbances.

6.5. Design and performance of nonlinear RC

The design steps in this section are illustrated for ILC, yet they can be applied almost directly to RC as is also summarized in Procedure 11. The three main differences are the following.

- Regarding the design of the filters L_R and Q_R (Section 6.2), the filters for repetitive control typically have finite preview which is compensated for in the delay D_N. In general, $L \approx T^{-1}$ is designed using ZPETC and Q is a FIR lowpass filter.
- Regarding the gains α and γ (Section 6.3), these are chosen similar to ILC using the corresponding convergence conditions from Theorem 8.
- Regarding the deadzone width (Section 6.4), similar data can be used to determine the deadzone width in RC, by measuring n_e

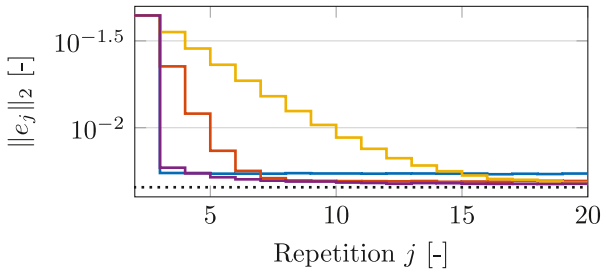

Fig. 18. Error 2-norm reduction over repetitions for repetitive control, averaged over 20 simulations. Compared to linear RC for $\alpha = 1$(—), 0.5 (—), and 0.2 (—), nonlinear RC with $\gamma = 1$, $\alpha = 0.1$ and $\delta = 2\times10^{-4}$ (—) achieves faster learning and lower errors. The noise floor (·····) follows from the averaged 2-norm of twenty noise realizations. RC is activated at repetition 2. (For interpretation of the references to color in this figure legend, the reader is referred to the web version of this article.)

repetitions with length N and taking

$$e_j = \begin{bmatrix} e((j-1)N+1) & \ldots & e(jN) \end{bmatrix}^{\mathsf{T}} \tag{28}$$

where N corresponds with the periodic disturbance.

Next, nonlinear repetitive control is applied to a simulated printer system, the carriage of which performs a periodic motion. The printer is modeled as a discrete-time non-collocated two-mass–spring–damper system. The system is sampled at $f_s = 1000$ Hz and the reference y_d leads to a disturbance that is periodic with $N = 2000$ such that $f_d = 0.5$ Hz. The non-periodic disturbance comes from zero-mean Gaussian white output noise $\tilde{v}$ with a variance of 10^{-8}. The learning filter L is constructed using ZPETC and the robustness filter Q is a 30th order zero-phase low-pass FIR filter (Longman, 2010) with a cut-off frequency of 200 Hz. Each simulation is repeated 20 times and averaged.

Based on the approach in Section 6.4, the deadzone width is set to $\delta = 2\times10^{-4}$. In Fig. 18 the error 2-norm over repetitions for nonlinear RC with $\gamma = 1$, $\alpha = 0.1$ is compared to linear RC with $\alpha = 1$, $\alpha = 0.5$ and $\alpha = 0.2$. Similar to linear ILC, smaller values of $0 < \alpha \leq 1$ lead to slower convergence and lower errors. The simulations illustrate that nonlinear RC converges fast to low errors, removing the trade-off between convergence speed and converged error value.

7. Experimental results

In this section, the presented approach is experimentally validated. It is shown that by using a deadzone in the learning filter in ILC and RC, the traditional trade-off between convergence speed and performance is removed.

7.1. Case 2: Nonlinear ILC on a prototype motion system

The presented approach is validated using a fourth-order mechatronic system consisting of two rotating masses connected by an axle that acts as a spring and damper, shown in Fig. 19. The system is measured at the mass that is not actuated directly, i.e., the system is non-collocated. The setup is placed in closed-loop with a feedback controller consisting of a notch filter, a low-pass filter and a lead–lag filter. Nonlinear parallel ILC is applied, see Fig. 3, such that the system J considered in the ILC procedures is the process sensitivity of the experimental setup. In Fig. 20 the measured frequency response of the process sensitivity as well as a model fitted on this data are shown. The third-order reference consists of a forward and backward rotation. Gaussian white noise with a variance of 0.002 is added to the plant input, resulting in the mean and noise estimates shown in Fig. 21.

Linear and nonlinear frequency-domain ILC are applied to the system, following the design procedure described in Section 6. Based on Fig. 21 a deadzone width of 0.04 is chosen. Learning filter L is designed

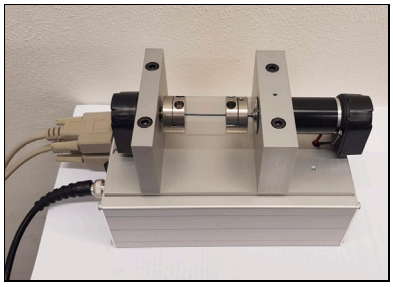

Fig. 19. Two mass–spring–damper system. The actuator is connected to the mass on the right, in the non-collocated situation the position of the mass on the left is controlled.

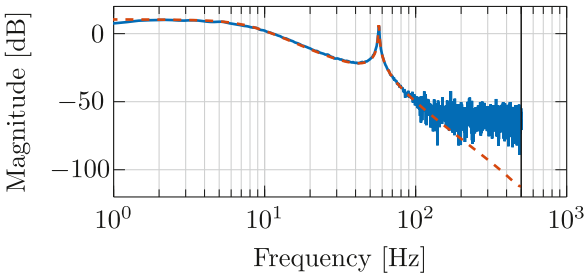

Fig. 20. Bode magnitude plot of the measured frequency response (—) and model (- -) of J for the two mass–spring–damper system in Fig. 19. (For interpretation of the references to color in this figure legend, the reader is referred to the web version of this article.)

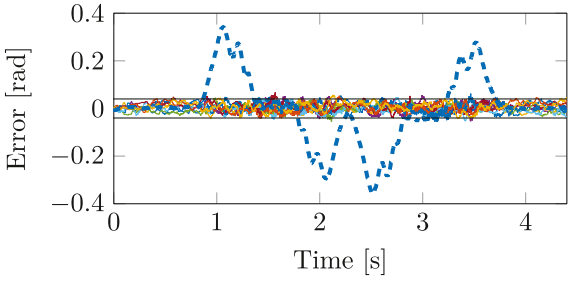

Fig. 21. Mean $\hat{r}$ of the error signal over 20 iterations (—) and the noise estimates $\hat{v}_j$ for $j = 1, 2, \ldots, 20$ for the two mass–spring–damper system. The black lines indicate the interval $[-0.04, 0.04]$, which encompasses most of the iteration-varying disturbances. (For interpretation of the references to color in this figure legend, the reader is referred to the web version of this article.)

using stable inversion, meaning that an exact non-causal inverse of the model shown in Fig. 20 is used. The robustness filter $Q = Q_p^* Q_p$ is zero-phase filter, with Q_p a second-order lowpass filter with a cutoff frequency of 70 Hz. The nonlinear gains for which the convergence condition is satisfied are given by $\gamma = 0.95$, $\alpha = 0.1$.

The error 2-norm over iterations for three different linear approaches as well as the presented nonlinear approach is shown in Fig. 22. For linear ILC, the trade-off between convergence speed and converged error is illustrated. A high learning gain $\alpha = 1$ results in fast convergence, while a lower learning gain $\alpha = 0.2$ results in much slower convergence, but the resulting error is reduced because iteration-varying disturbances are less amplified. Nonlinear ILC combines the advantages, achieving both fast convergence and a small converged error, thus removing the trade-off.

7.2. Case 3: Nonlinear RC on an industrial print belt system

Nonlinear repetitive control is applied to an industrial print belt system, shown in Fig. 23. The aim of the system is to transport paper

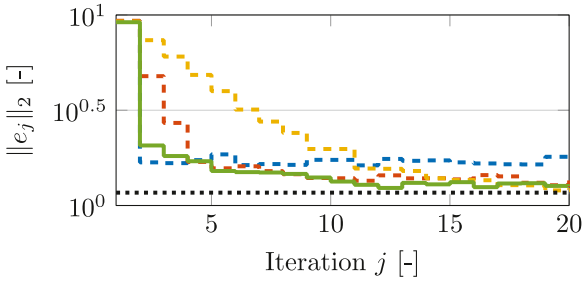

Fig. 22. Error 2-norm for linear ILC with $\alpha = 1$ (- -), 0.5 (- -) and 0.2 (- -) and nonlinear ILC with $\alpha = 0.1$, $\gamma = 0.95$ and $\delta = 0.04$ (—), applied to the two mass–spring–damper system. The noise floor (·····) follows from the averaged 2-norm of ten noise realizations. Nonlinear ILC removes the trade-off between convergence speed and converged error. (For interpretation of the references to color in this figure legend, the reader is referred to the web version of this article.)

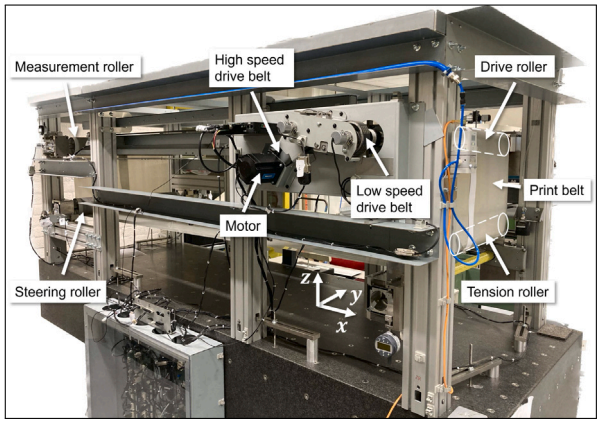

Fig. 23. Industrial print belt system. The aim is to transport paper on the print belt with a constant velocity. The rollers and drive belts induce various repeating disturbances in the system.

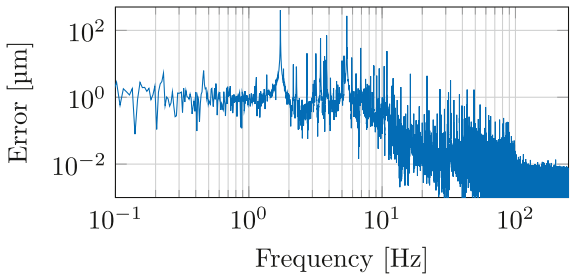

Fig. 24. Error spectrum of the print belt system without RC. The disturbances due to the low-speed and high-speed drive belts are visible at respectively 1.7 Hz and 5.4 Hz.

on the print belt with a constant velocity, during which the rollers and drive belts introduce repeating disturbances at various frequencies. Linear and nonlinear repetitive controllers are applied to attenuate the disturbances originating from the low-speed and high-speed drive belts, which occur at respectively 1.7 Hz and 5.4 Hz as shown in Fig. 24.

The disturbance caused by the low-speed drive belt is attenuated using standard RC with $\alpha = 0.1$. For the high-speed drive belt, different configurations are compared. To ensure stability and safe operation of the system, the sum of the learning gains α and γ for the high-speed drive belt is limited to 0.3. The error and cumulative error spectra for linear RC with $\alpha = 0.1$ and $\alpha = 0.2$ and nonlinear RC with $\alpha = 0.05$, $\gamma = 0.2$ and $\delta = 1 \times 10^{-4}$ are shown in Fig. 25. All RC implementations strongly reduce the disturbances at 1.7 Hz and 5.4 Hz. Because there is limited room for large learning gains in the safe

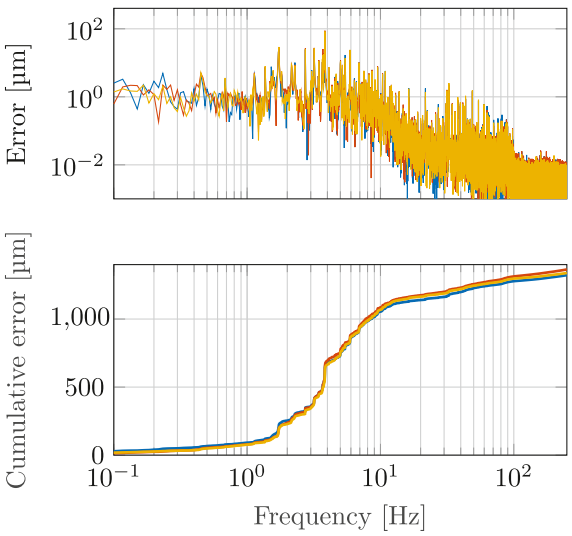

Fig. 25. Error spectrum (top) and cumulative error spectrum (bottom) of 60 s of steady-state operation of the print belt system with linear RC to compensate the disturbance from the low-speed drive belt (1.7 Hz). The disturbance from the high-speed drive belt (5.4 Hz) is compensated using linear RC with $\alpha = 0.1$ (—) and $\alpha = 0.2$ (—), and nonlinear RC with $\alpha = 0.05$, $\gamma = 0.2$ and $\delta = 1 \times 10^{-4}$ (—). All approaches compensate the disturbance at 5.4 Hz well (cf. Fig. 24) and since all approaches use comparable low learning gains, the performance is similar. (For interpretation of the references to color in this figure legend, the reader is referred to the web version of this article.)

learning range, all approaches use comparable learning gains that lead to similar converged errors, which are as small as possible. Showing the convergence speed similar to the simulation results in Fig. 18 is complicated in practice, because the system is operating continuously. However, the results demonstrate that nonlinear ILC indeed leads to a stable system and good compensation of repeating disturbances. In addition, Fig. 25 shows that for similar learning gains and convergence speeds, nonlinear RC with $\gamma = 0.2$, $\alpha = 0.05$ obtains a slightly smaller error than linear RC with $\alpha = 0.2$.

8. Conclusions

Nonlinear frequency-domain ILC and RC algorithms are developed that achieve both fast convergence and a small converged error in the presence of non-repeating disturbances. The approach removes the traditional trade-off between convergence speed and limited amplification of non-repeating disturbances by applying various learning gains to different elements of the error signal depending on their magnitude. A condition for monotonic convergence of the frequency-domain algorithm is given, which is reminiscent of the existing convergence criterion for frequency-domain ILC and which can be evaluated using measured frequency-response data of the system. For RC, a stability condition is developed by interpreting the system as a convergent Lur'e system. A design procedure based on disturbance measurements and system knowledge is provided. The effect of the various design parameters is illustrated using simulations, and both nonlinear ILC and nonlinear RC are validated in simulations and experiments in which fast convergence to small errors is demonstrated. Future research should involve the analysis of the effect of the design parameters in nonlinear ILC and RC on the converged error, similar to the analysis in Section 5.1.

CRediT authorship contribution statement

Leontine Aarnoudse: Writing – review & editing, Writing – original draft, Validation, Investigation, Formal analysis, Conceptualization. **Alexey Pavlov:** Writing – review & editing, Supervision, Investigation, Formal analysis, Conceptualization. **Tom Oomen:** Writing – review & editing, Supervision, Investigation, Funding acquisition, Formal analysis, Conceptualization.

Declaration of competing interest

The authors declare that they have no known competing financial interests or personal relationships that could have appeared to influence the work reported in this paper.

Acknowledgment

The authors thank Kevin Cox and Sjirk Koekebakker for their contributions to the repetitive control experiments.

Appendix

Proof of Theorem 4

In this section, the proof of Theorem 4 is provided. The following auxiliary lemma is used in this proof.

Lemma 12. *After a loop transformation, the feedforward update with $\varphi(e_j)$ satisfying sector condition (4) is equivalent to*

$$f_{j+1} = Q\left(f_j + \left(\alpha + \frac{\gamma}{2}\right) Le_j + L\tilde{\varphi}(e_j)\right), \tag{29}$$

$$\tilde{\varphi}(e_j) = \varphi(e_j) - \frac{\gamma}{2} e_j \tag{30}$$

with nonlinearity $\tilde{\varphi}(e_j)$ satisfying the symmetric sector condition

$$-\frac{\gamma}{2} \leq \frac{\tilde{\varphi}(e_1) - \tilde{\varphi}(e_2)}{e_1 - e_2} \leq \frac{\gamma}{2}. \tag{31}$$

Proof of Theorem 4. Consider two solutions e_1 and e_2 to (7), with the same iteration-varying input $(\alpha + \frac{\gamma}{2})QL(S(y_d - v_j))$. Substitution in condition (9) for $P = I$ gives

$$\begin{aligned} &\|h(e_1, j) - h(e_2, j)\|_2 = \\ &\quad \|Q(1 - \alpha JL)(e_1 - e_2) - QJL(\varphi(e_1) - \varphi(e_2))\|_2. \end{aligned} \tag{32}$$

Using the loop transformation of Lemma 12,

$$\begin{aligned} \|h(e_1, j) - h(e_2, j)\|_2 &= \| Q\left(1 - \left(\alpha + \frac{\gamma}{2}\right) JL\right)(e_1 - e_2) \\ &\qquad - QJL(\tilde{\varphi}(e_1) - \tilde{\varphi}(e_2)) \|_2 \\ &\leq \left\| Q\left(1 - \left(\alpha + \frac{\gamma}{2}\right) JL\right)(e_1 - e_2) \right\|_2 \\ &\quad + \left\| QJL(\tilde{\varphi}(e_1) - \tilde{\varphi}(e_2)) \right\|_2, \\ &\leq \left\| Q\left(1 - \left(\alpha + \frac{\gamma}{2}\right) JL\right) \right\|_{\mathcal{L}_\infty} \|e_1 - e_2\|_2 \\ &\quad + \|QJL\|_{\mathcal{L}_\infty} \left\|\tilde{\varphi}(e_1) - \tilde{\varphi}(e_2)\right\|_2, \end{aligned} \tag{33}$$

through application of the triangle inequality and multiplicative property for matrix norms, and Zhou, Doyle, and Glover (1996, Theorem 4.4). From (31), it follows that for each entry of e_1 and e_2,

$$|\tilde{\varphi}(e_1(k)) - \tilde{\varphi}(e_2(k))| \leq \frac{\gamma}{2} |e_1(k) - e_2(k)|. \tag{34}$$

Therefore, it also holds that

$$\|\tilde{\varphi}(e_1) - \tilde{\varphi}(e_2)\|_2 \leq \frac{\gamma}{2} \|e_1 - e_2\|_2. \tag{35}$$

Using this inequality,

$$\begin{aligned} &\|h(e_1, j) - h(e_2, j)\|_2 \\ &\leq \left\| Q\left(1 - \left(\alpha + \frac{\gamma}{2}\right) JL\right) \right\|_{\mathcal{L}_\infty} \|e_1 - e_2\|_2 \end{aligned}$$

$$+ \frac{\gamma}{2}\|QJL\|_{\mathcal{L}_\infty}\|e_1 - e_2\|_2 \tag{36}$$
$$\leq \left(\left\|Q\left(1-\left(\alpha+\frac{\gamma}{2}\right)JL\right)\right\|_{\mathcal{L}_\infty}+\frac{\gamma}{2}\|QJL\|_{\mathcal{L}_\infty}\right)\|e_1-e_2\|_2$$

It follows that condition (9) with $P = I$ holds for (7) if

$$\left\|Q\left(1-\left(\alpha+\frac{\gamma}{2}\right)JL\right)\right\|_{\mathcal{L}_\infty}+\frac{\gamma}{2}\|QJL\|_{\mathcal{L}_\infty} \leq \rho \tag{37}$$

with $\rho < 1$. □

Proof of Theorem 8

In this section, the proof of Theorem 8 is provided. The following auxiliary lemma for the cascade of two exponentially convergent systems (Aarnoudse, Pavlov, Kon, & Oomen, 2023, Lemma 4) is used in the proof.

Lemma 13. *Consider the cascaded system*

$$\begin{cases} x(k+1) = f(x(k), w(k), k) \\ w(k+1) = g(w(k), k). \end{cases} \tag{38}$$

Suppose the x-subsystem meets the conditions in Lemma 2 for any $w(k)$ bounded on $\mathbb{Z}$ and is therefore exponentially convergent, and the w-subsystem is exponentially convergent. In addition, $f(x, w, k)$ is globally Lipschitz with respect to w with Lipschitz constant K, i.e.,

$$\|f(x, w_1, k) - f(x, w_2, k)\| \leq K\|w_1 - w_2\| \forall x, k. \tag{39}$$

Then system (38) is exponentially convergent.

Proof of Theorem 8. Consider system (19) as a cascade of (19a) and (19b). The idea is to establish exponential convergence as a cascade of two exponentially convergent systems. First, condition (a) ensures that system (19b) is exponentially convergent for any bounded input $e_0(k)$, as a linear exponentially stable system. Secondly, the incremental sector condition in (b) ensures that the right-hand side of (19a) is globally Lipschitz in w, uniformly in x, i.e., that (39) holds. Thirdly, conditions (a) -(c) ensure that the nonlinear Lur'e system (19a) with $w(k)$ as inputs is convergent. Condition (9) of Lemma 2 is applied to the Lur'e system (19a). Take

$$f(x_1, k) - f(x_2, k) = A\Delta x - B\Delta\varphi, \tag{40}$$

with $\Delta x = x_1 - x_2$ and $\Delta\varphi = \varphi(Cx_1 + w(k)) - \varphi(Cx_2 + w(k))$. Using (40), condition (9) is rewritten to

$$\begin{bmatrix}\Delta x \\ \Delta\varphi\end{bmatrix}^\mathsf{T}\begin{bmatrix}A^\mathsf{T}PA & -A^\mathsf{T}PB \\ -B^\mathsf{T}PA & B^\mathsf{T}PB\end{bmatrix}\begin{bmatrix}\Delta x \\ \Delta\varphi\end{bmatrix} - \lambda^2\Delta x^\mathsf{T}P\Delta x \leq 0,\ \forall x_1, x_2 \in \mathbb{R}^n, k \in \mathbb{Z}. \tag{41}$$

Next, the incremental sector condition (4) for φ is written as a quadratic matrix inequality for $\Delta\varphi$. Denote $z_i = Cx_i + w(k)$ and $\Delta z = z_1 - z_2$. By condition (b) , φ satisfies the incremental sector condition with γ, and therefore

$$\begin{bmatrix}\Delta z \\ \Delta\varphi\end{bmatrix}^\mathsf{T}\begin{bmatrix}\gamma^2 & 0 \\ 0 & -1\end{bmatrix}\begin{bmatrix}\Delta z \\ \Delta\varphi\end{bmatrix} \geq 0. \tag{42}$$

Substituting $\Delta z = C\Delta x$ and dividing by γ^2 gives

$$\begin{bmatrix}\Delta x \\ \Delta\varphi\end{bmatrix}^\mathsf{T}\begin{bmatrix}C^\mathsf{T}C & 0 \\ 0 & -\frac{1}{\gamma^2}\end{bmatrix}\begin{bmatrix}\Delta x \\ \Delta\varphi\end{bmatrix} \geq 0. \tag{43}$$

The system is exponentially convergent if there exists $P = P^\mathsf{T} \succ 0$ and $\lambda \in (0, 1)$ such that (41) holds for all $\Delta x, \Delta\varphi$ that satisfy (43). By the S-procedure (Pólik & Terlaky, 2007), this holds if there exists a $P = P^\mathsf{T} \succ 0$, $\lambda \in (0, 1)$ such that

$$\begin{bmatrix}\Delta x \\ \Delta\varphi\end{bmatrix}^\mathsf{T}\begin{bmatrix}A^\mathsf{T}PA + C^\mathsf{T}C - \lambda^2 P & -A^\mathsf{T}PB \\ -B^\mathsf{T}PA & B^\mathsf{T}PB - \frac{1}{\gamma^2}\end{bmatrix}\begin{bmatrix}\Delta x \\ \Delta\varphi\end{bmatrix}$$
$$\leq 0,\ \forall x_1, x_2 \in \mathbb{R}^n, k \in \mathbb{Z}. \tag{44}$$

Taking $\lambda^2 = 1 - \varepsilon$ for some $\varepsilon \in (0, 1)$ in (44) gives

$$\begin{bmatrix}\Delta x \\ \Delta\varphi\end{bmatrix}^\mathsf{T}\begin{bmatrix}A^\mathsf{T}PA + C^\mathsf{T}C - P & -A^\mathsf{T}PB \\ -B^\mathsf{T}PA & B^\mathsf{T}PB - \frac{1}{\gamma^2}\end{bmatrix}\begin{bmatrix}\Delta x \\ \Delta\varphi\end{bmatrix} + \Delta x^\mathsf{T}\varepsilon P\Delta x \leq 0,\ \forall x_1, x_2 \in \mathbb{R}^n, k \in \mathbb{Z}. \tag{45}$$

If there exists a $P = P^\mathsf{T} \succ 0$ such that the strict inequality

$$\begin{bmatrix}\Delta x \\ \Delta\varphi\end{bmatrix}^\mathsf{T}\begin{bmatrix}A^\mathsf{T}PA + C^\mathsf{T}C - P & -A^\mathsf{T}PB \\ -B^\mathsf{T}PA & B^\mathsf{T}PB - \frac{1}{\gamma^2}\end{bmatrix}\begin{bmatrix}\Delta x \\ \Delta\varphi\end{bmatrix} < 0,\ \forall x_1, x_2 \in \mathbb{R}^n, k \in \mathbb{Z}, \tag{46}$$

holds, then there also exists $\varepsilon \in (0, 1)$ such that nonstrict inequality (45) holds for the same P, and consequently (44) holds for the same P and $\lambda = \sqrt{1-\varepsilon} \in (0, 1)$. By the Kalman-Szegö lemma, see, e.g., Matveev and Pogromsky (2016, Lemma 17), a matrix $P = P^\mathsf{T} \succ 0$ for which (46) holds exists if and only if

$$\|-T_R\|_\infty = \|T_R\|_\infty = \sup_{\omega\in[0,2\pi)}|T_R(e^{i\omega})| < \frac{1}{\gamma}, \tag{47}$$

which is ensured by condition (c) . It follows that if conditions (a) -(c) are satisfied, then system (19a) is exponentially convergent for any bounded $w(k)$ by Lemma 13. □

References

Aarnoudse, L., Pavlov, A., Kon, J., & Oomen, T. (2023). Nonlinear Repetitive Control for Mitigating Noise Amplification. In *Conf. decis. control* (pp. 2891–2896).

Aarnoudse, L., Pavlov, A., & Oomen, T. (2023a). Nonlinear iterative learning control: a frequency-domain approach for fast convergence and high accuracy. In *2023 IFAC world congr.* (pp. 1889–1894).

Aarnoudse, L., Pavlov, A., & Oomen, T. (2023b). Nonlinear iterative learning control for discriminating between disturbances. (submitted).

Blanken, L., Koekebakker, S., & Oomen, T. (2020). Multivariable Repetitive Control: Decentralized Designs with Application to Continuous Media Flow Printing. *IEEE/ASME Transactions on Mechatronics*, *25*(1), 294–304.

Bristow, D. A., Tharayil, M., & Alleyne, A. G. (2006). A survey of iterative learning control. *IEEE Control Systems*, *26*(3), 96–114.

Butcher, M., Karimi, A., & Longchamp, R. (2008). A statistical analysis of certain iterative learning control algorithms. *International Journal of Control*, *81*(1), 156–166.

Chang, W. S., Suh, I. H., & Kim, T. W. (1995). Analysis and design of two types of digital repetitive control systems. *Automatica*, *31*(5), 741–746.

Chen, H. (2003). Almost sure convergence of iterative learning control for stochastic systems. *Science in China, Series F*, *46*(1), 67–79.

Chen, X., & Tomizuka, M. (2014). New repetitive control with improved steady-state performance and accelerated transient. *IEEE Transactions on Control Systems Technology*, *22*(2), 664–675.

De Roover, D., Bosgra, O. H., & Steinbuch, M. (2000). Internal-model-based design of repetitive and iterative learning controllers for linear multivariable systems. *International Journal of Control*, *73*(10), 914–929.

Deutschmann-Olek, A., Stadler, G., & Kugi, A. (2021). Stochastic Iterative Learning Control for Lumped-and Distributed-Parameter Systems: A Wiener-Filtering Approach. *IEEE Transactions on Automatic Control*, *66*(8), 3856–3862.

Gunnarsson, S., & Norrlöf, M. (2001). On the design of ILC algorithms using optimization. *Automatica*, *37*(12), 2011–2016.

Heertjes, M., & Steinbuch, M. (2004). Stability and performance of a variable gain controller with application to a dvd storage drive. *Automatica*, *40*(4), 591–602.

Heertjes, M., & Tso, T. (2007). Nonlinear iterative learning control with applications to lithographic machinery. *Control Engineering Practice*, *15*(12), 1545–1555.

Khalil, H. K. (2002). *Nonlinear systems* (3rd ed.). New Jersey: Prentice Hall.

Ljung, L. (1999). *System identification* (2nd ed.). Upper Saddle River, NJ: Prentice Hall.

Longman, R. W. (2000). Iterative learning control and repetitive control for engineering practice. *International Journal of Control*, *73*(10), 930–954.

Longman, R. W. (2010). On the theory and design of linear repetitive control systems. *European Journal of Control*, *16*(5), 447–496.

Matveev, A., & Pogromsky, A. (2016). Observation of nonlinear systems via finite capacity channels: Constructive data rate limits. *Automatica*, *70*, 217–229.

Oomen, T. (2020). Learning for Advanced Motion Control. In *IEEE int. work. adv. motion control*.

Oomen, T., & Rojas, C. R. (2017). Sparse iterative learning control with application to a wafer stage: Achieving performance, resource efficiency, and task flexibility. *Mechatronics*, *47*, 134–147.

Pavlov, A., Hunnekens, B. G., Wouw, N. V., & Nijmeijer, H. (2013). Steady-state performance optimization for nonlinear control systems of Lur'e type. *Automatica*, *49*(7), 2087–2097.

Pavlov, A., & Van De Wouw, N. (2012). Steady-state analysis and regulation of discrete-time nonlinear systems. *IEEE Transactions on Automatic Control*, *57*(7), 1793–1798.

Pipeleers, G., Demeulenaere, B., De Schutter, J., & Swevers, J. (2008). Robust high-order repetitive control: Optimal performance trade-offs. *Automatica*, *44*(10), 2628–2634.

Pólik, I., & Terlaky, T. (2007). A Survey of the S-Lemma. *SIAM Review*, *49*(3), 371–418.

Saab, S. S. (2001). On a discrete-time stochastic learning control algorithm. *IEEE Transactions on Automatic Control*, *46*(8), 877–887.

Saab, S. S. (2003). Stochastic P-type/D-type iterative learning control algorithms. *International Journal of Control*, *76*(2), 139–148.

Shen, D., & Wang, Y. (2014). Survey on stochastic iterative learning control. *Journal of Process Control*, *24*(12), 64–77.

Sogo, T. (2010). On the equivalence between stable inversion for nonminimum phase systems and reciprocal transfer functions defined by the two-sided Laplace transform. *Automatica*, *46*(1), 122–126.

Steinbuch, M., Weiland, S., & Singh, T. (2007). Design of noise and period-time robust high-order repetitive control, with application to optical storage. *Automatica*, *43*(12), 2086–2095.

Tomizuka, M. (1987). Zero phase error tracking algorithm for digital control. *Journal of Dynamic Systems, Measurement and Control*, *109*, 65–68.

Yeol, J. W., & Longman, R. W. (2008). Time and frequency domain evaluation of settling time in repetitive control. In *AIAA/AAS astrodyn. spec. conf. exhib.*.

Zhou, K., Doyle, J. C., & Glover, K. (1996). *Robust and optimal control*. Englewood Cliffs, New Jersey: Prentice Hall.